Corrosion front roughening in two-dimensional pitting of aluminum thin layers

László Balázs*
CNRS–Laboratoire de Physique de la Matière Condensée Ecole Polytechnique, Palaiseau, 91128, France
(Received 21 February 1996)

A smooth to fractal transition of the corrosion front has been observed during two-dimensional pitting of Al thin films. The propagation of the initially smooth front ceased spontaneously, leaving behind a self-similar coastline with fractal dimension $D_f=1.33\pm0.01$. The roughening transition can be interpreted within the framework of the spreading bond percolation model with trapping. Quantitative agreement has been found between model calculations and the dynamic exponents characterizing the temporal behavior of the propagation velocity as well as the roughness of the front. [S1063-651X(96)00208-5]

PACS number(s): 64.60.Ak

INTRODUCTION

Considerable interest is shown in the formation and propagation of rough interfaces [1,2]. In this respect, pitting corrosion [3] attracted significant attention because of the challenging problem in the development of irregular corrosion holes observed in bulk metals [3,4]. Despite substantial theoretical efforts [5–8], the formation mechanism of these corrosion structures is still not clear. There are two major obstacles to a better understanding of pit growth: problems concerning the characterization of three-dimensional (3D) morphologies, and the lack of detailed information on the dynamics of pit evolution in bulk metals.

The study of two-dimensional corrosion structures has proved to be advantageous since the corrosion front is easily detectable and directly accessible to image analysis. The morphology of 2D patterns can be precisely characterized.

Holten *et al.* [9] carried out potentiostatic corrosion measurements on 50-μm-thick aluminum foils glued between two glass plates. They analyzed the morphology of the corrosion front by different methods and showed that fronts can be described in terms of self-affine geometry. Frankel [10] studied potentiostatically controlled pit growth in thin Al films. Convoluted pit perimeters were observed close to the threshold pitting potential but the morphology of pits was not analyzed in detail.

A rich variety of morphologies has been observed in the open-circuit pitting of evaporated Al thin layers in NaCl and $Fe_2(SO_4)_3$ containing acidic medium [11]. It was shown that the shape of the corrosion patterns depends on the layer thickness, the *p*H, the concentration of aggressive anions (Cl^-) as well as the concentration of the given oxidizing agent (Fe^{3+}).

The evolution of *entire* two-dimensional pits in Al films was studied in an earlier publication [12]. Dissolution of the metal takes place locally, exclusively at individual growth sites of approximately the same size scattered along the pit perimeter. As the growth sites advance channels with walls perpendicular to the glass substrate are etched in the metal layer. While side walls of the channels become passive (i.e., they are covered with aluminum oxide, which prevents the vigorous reaction between the metal and the electrolyte), the active channel tips (the growth sites) propagate randomly in the two-dimensional aluminum layer. During their motion active sites cut the metal film into pieces, thus trapping aluminum islands of various sizes within the two-dimensional pit [11]. The stability of the evolving channel tips against passivation increases with the local accumulation of corrosion products. The morphology of 2D pits growing under open circuit conditions is influenced by large local fluctuation of electrolyte composition due to intensive hydrogen bubbling at the anodic active sites and the global constraint on the corrosion current imposed by the cathodic reactions taking place on the oxide covered passive metal surface [12]. The various 2D pit morphologies can be understood by means of a simple growth model based on the above assumptions. The overall pit morphology is basically determined by the size and the number of propagating active sites. It has been shown that as long as the propagation of growth sites is not correlated and their number is not limited this model is equivalent to spreading bond percolation with trapping [12].

In the relatively high Fe^{3+} concentration range the development of patterns with ''mixed'' morphology is observed [11,12]. In this case growth sites are not randomly scattered along the pit perimeter. Some of them coalesce, producing long smooth fronts whereas at other parts rugged interfaces are formed as a consequence of random propagation of individual channels. In the case of ''mixed'' patterns it is straightforward to divide the pit perimeter into subsections with more or less uniform morphology. Instead of dealing with the development of the entire corrosion pattern, the evolution of different perimeter sections (corrosion fronts with distinct morphologies) is characterized separately. There is another, practical argument in favor of the local characterization of pit evolution: as the pattern increases and the magnification of the image is decreased to keep the whole pattern in the observation field of the microscope, important details are lost due to the finite resolution of the video camera.

Depending on the experimental conditions the morphology of the propagating corrosion front may change in time. Gradual or sudden roughening of the previously smooth

*On leave from KFKI-Institute for Atomic Energy Research, P.O.B. 49, H-1525 Budapest (Hungary). Present address: GE Lighting Tungsram, Bródy Research Center-321, Váci út 77, Budapest H-1340, (Hungary). Electronic address: balazs%t1@dess0.light.ge.com

front often occurs. Spontaneous morphological changes indicate unstable growth and the evolution of the corrosion front may cease ending in a convoluted, fractal-like pit perimeter.

A phenomenological description of the two-dimensional corrosion front development and roughening is still lacking. Although several models have been published dealing with the formation of rough and smooth corrosion walls [6–8], none of them can be reconciled with the aforementioned observations. Here we are concerned with the dynamics of two-dimensional corrosion front development and roughening in Al thin films. The results of an experiment are presented in which the gradual roughening of an initially smooth corrosion front was observed. Both the dynamic and the static critical exponents are determined in order to characterize the front development and front roughness, respectively. The quantitative agreement with calculations based on the spreading bond percolation model with trapping reveals that corrosion front roughening can be interpreted within the framework of spreading percolation phenomena.

EXPERIMENT

A 31-nm-thick aluminum film evaporated onto an optically flat glass substrate was used. The sample was immersed into an electrolyte containing 0.5 m*M* $Fe_2(SO_4)_3$, 5 m*M* HCl, 10 m*M* Na_2SO_4, and 5 m*M* NaCl. The evolution of one single pit was observed by means of a charge-coupled device camera attached to a microscope. The specimen was inspected in transmitted light and the video signal was recorded on tape. Special attention has been devoted to attain uniform illumination of the specimen. The resulting video images taken of the 1.64 mm×1.09 mm area of the specimen have been digitized into 8-bit gray-scale pictures containing 768×512 pixels. In a separate experiment the propagation of the rough corrosion front was recorded with 4 times higher magnification.

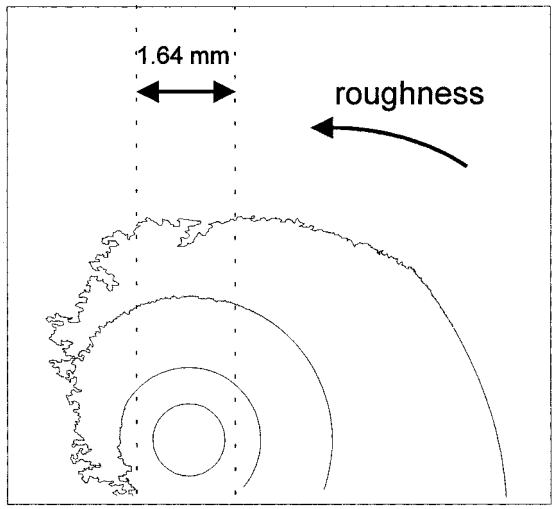

FIG. 1. Different stages of two-dimensional pit growth in Al film (schematic view). Dotted lines show the width of the microscopic observation. Temporal roughening leading to the cessation of front development within this band was recorded on video tape. A continuous transition from the smooth to the rough coastline along the pit perimeter was observed after the pit evolution was stopped by flooding the cell with distilled water.

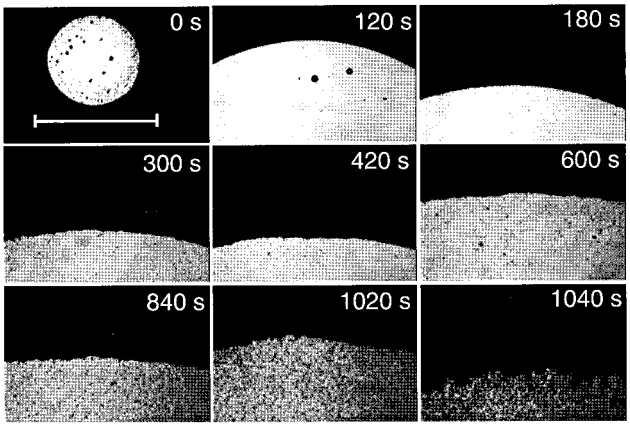

FIG. 2. Sequence of video images (in transmitted light) taken from different stages of the evolving corrosion front. The scale bar in the upper left illustration corresponds to 1 mm.

RESULTS AND DISCUSSION

The pit perforated the thin metal layer and it grew by dissolution of aluminum from the active pit wall perpendicular to the glass substrate. Figure 1 shows a schematic view of the pit growth in the aluminum film. Initially a circular hole was observed, which became elongated at a later stage of the growth after the pit perimeter reached the sample border. The local morphology of the evolving pit perimeter changed gradually from smooth to rough. Dissolution stopped where the most convoluted, fractal-like perimeter section was formed. Propagation of the corrosion front was followed in a 1.64-mm-wide band, which was sufficiently narrow to ensure that the morphology of the perimeter section studied was always uniform and therefore it could be characterized by a single roughness parameter. Our results concern the temporal changes in the morphology of this part of the pit perimeter.

In Fig. 2 a sequence of video images taken of the corrosion front evolving in the 1.64-mm broad band is presented. At the beginning of the growth hydrogen bubbles (dark spots) were formed in the interior of the circular pit and they then became attached to the glass substrate. As time passed, the size of the hole increased, and the propagation velocity of the front decreased. At about 180 s the corrosion front be-

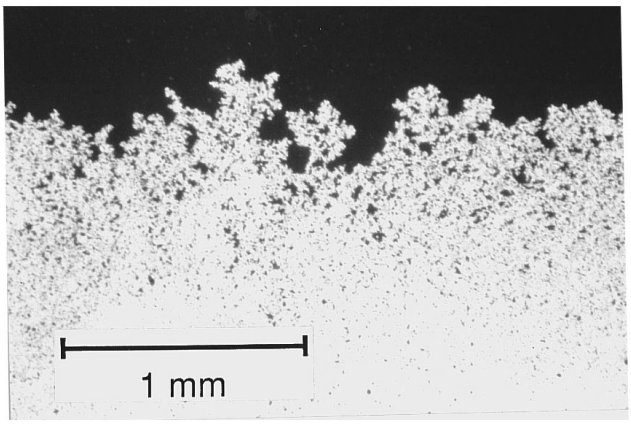

FIG. 3. Photo of the corrosion front investigated (cf. Fig. 1) after its propagation has ceased spontaneously.

came slightly ramified and tiny aluminum islands remained, which reduced the transmittance of the region behind the front. The roughening of the pit perimeter indicated that the corrosion front had been locally passivated on certain spots. The irregularity of the corrosion front steadily increased. After 1000 s an abrupt change started in the front morphology and metal dissolution ceased at the investigated front section.

Figure 3 shows a photo of the spontaneously stopped fractal front. The photo has been digitized into a 1720×795 black and white pixel image. The front, i.e., set of black pixels having at least one white neighbor and connected to the unattacked Al layer, has been traced and is shown in the upper section of Fig. 4. We used the box counting method [1] to determine the fractal dimension of the irregular coastline. As shown in Fig. 4, scaling with the exponent of 1.33 ±0.01 was found between 10 and 1000 μm.

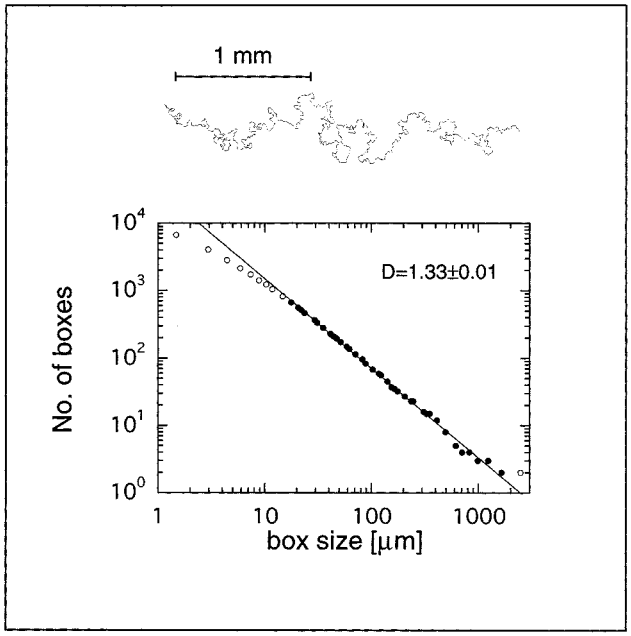

FIG. 4. Result of box counting analysis for the experimentally observed corrosion front (cf. Fig. 3) shown in the upper part of the figure. The straight line corresponds to a power function fitted to the data points. Fractal dimension of the front was found to be 1.33 ±0.01.

A. Rough front propagation studied with higher magnification

Since the resolution of the video images shown in Fig. 2 was not sufficiently good to allow detailed analysis of the rough front propagation, in a separate experiment the evolution of the rough pit perimeter was recorded with four times higher magnification compared to the previous pictures shown in Fig. 1. The sequence of images captured with 1-s sampling time is shown in Fig. 5. Evolution of individual channels is clearly resolved here. White arrows indicate the active regions where growth sites advance. Comparison of Figs. 5(d) and 5(e) shows the fate of active sites on a peninsula that is being transformed to an island. As the active sites continue to propagate and the island becomes formed the dissolution immediately stops on it. This feature resembles trapping introduced in invasion percolation phenomena [13].

In Figs. 5(a)–5(f) the salient characteristics of spreading percolation [1,14] are clearly seen: Dissolution is observed to take place only through individual active sites, which propagate randomly by etching channels of about 1-μm width into the metal layer (see regions indicated by arrows). Some channels stop growing; some of them bifurcate or split into several branches. Once the corrosion has ceased at a certain spot of the pit perimeter the metal dissolution never starts anew at that site. Although it is assumed that the local electrolyte composition determines whether the active tip of a channel becomes completely passive or the dissolution continues further, the fate of an individual active site appears to be completely random to the observer. Therefore active sites on a section of the corrosion front with uniform morphology can be treated as a statistical ensemble characterized by one single ''spreading probability.''

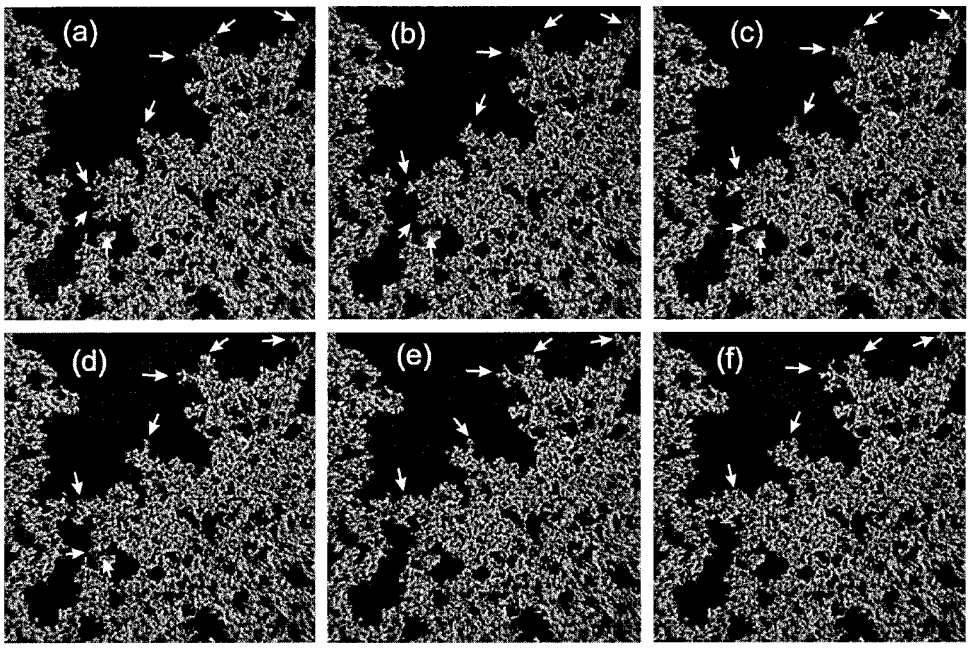

FIG. 5. Sequence of video images taken of the evolution of a rough corrosion front in transmitted light. The width of an image corresponds to 286 μm. White arrows indicate growth regions. Comparison of the images (d) and (e) reveals that metal dissolution stops on the newly formed metal island.

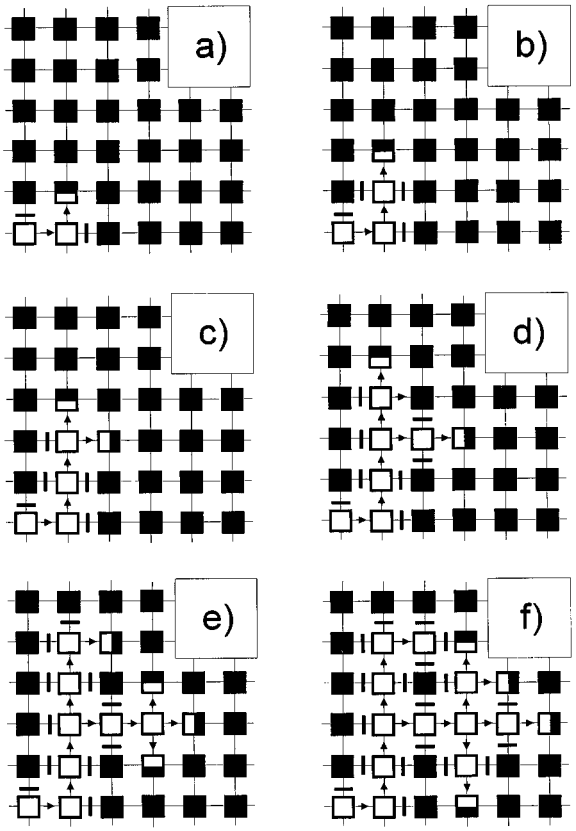

FIG. 6. Spreading bond percolation model of corrosion front propagation. Black and white squares stand for intact and dissolved sites, respectively. Active sites are indicated by semifilled squares. Arrows represent occupied bonds, black bars show blocked bonds.

B. The model

The propagation of the growth sites can be interpreted by means of a model incorporating the features of spreading percolation supplemented with the phenomenon of trapping to account for the experimentally observed conservation of metal islands. Figure 6 explains the growth rules of the model on a square lattice: At the beginning lattice sites are intact (black), representing microscopic ($\sim 1\ \mu\text{m} \times 1\ \mu\text{m}$) sections of the aluminum film connected by empty bonds (straight lines). The actual active sites (semifilled squares) can activate their undissolved nearest neighbors via empty bonds with spreading probability, p. In this case the bond connecting the active site to the intact site is occupied (arrow) and the site to which the arrow points will be activated. In the opposite case (occurring with probability $1-p$), the bond will be blocked (bar crossing the bond) and in this step the neighbor remains intact. With the next step the previously active (semifilled) sites turn white, i.e., ''aluminum is completely dissolved'' and active sites are advanced to the shell of the previous nearest neighbors. Trapping in the model means that on a newly formed island all the bonds connecting active and intact sites are blocked. Active sites become white without the possibility of neighbor activation.

The spreading probability determines the morphology of the advancing front. If p is close to 1, a steadily growing smooth front propagates. With the decrease of p the front becomes rougher and rougher and metal islands with increasing size are left behind the advancing front. When the spreading probability approaches the bond percolation threshold $p_c = 0.5$ [1,14], the front evolution arrives in the critical region and at p_c, the front stops.

C. Analysis of front roughening

The low resolution of video images (see Fig. 2) meant that the temporal behavior of individual growth sites could not be exactly characterized nor could the spreading probability associated with the front section studied be directly estimated. Instead we employed an indirect method to describe the morphological transition. The velocity and the roughness of the advancing front are uniquely determined by the spreading probability; consequently, from the temporal behavior of the propagation velocity and the front roughness the time dependence of p can be obtained. Instead of the direct morphological characterization of the advancing front (which would require the analysis of high-resolution images) we determined the transmittance of the corroded Al film adjacent to the front since the undissolved metal islands (their density and size distribution) can be regarded as the footprint of the advancing pit perimeter. The local transmittance is characteristic of the roughness of the front after it has passed over the region investigated. Therefore the dynamics of the morphological transition was described in terms of both the time-dependent transmittance and propagation velocity. From the analysis of these two quantities the history of the spreading probability can be obtained.

The transmittance of the corroded film, $T(t)$, was determined in a box of 400×100 pixels adjacent to the front. By means of an image analysis program the average gray value $G(t)$ was measured and the transmittance was calculated by

$$T(t) = \frac{G_{\max} - G(t)}{G_{\max} - G_{\min}}, \tag{1}$$

where $G_{\max}$ and $G_{\min}$ correspond to the maximum and minimum gray values measured over unattacked and Al-free domains, respectively. Due to the not perfectly uniform illumination of the specimen the measured transmittance slightly depended on the exact position of the measuring box. The accuracy of measurement decreased with the increasing size of the aluminum islands, but even in this case the scatter of measured transmittances was within 15%. This was checked by comparing transmittances obtained from successive video images captured within a 5-s interval.

In order to determine the propagation velocity, $v(t)$ of the growing front, a series of five images was digitized with 1-s time lag at various stages of the pit development. The average position of the front was plotted as a function of time and v was defined as the slope of the straight line fitted to the data points.

Figure 7 shows the temporal behavior of $v(t)$ and $T(t)$. An undershoot occurred between 200 and 400 s and, following this period, both quantities gradually decreased until a sharp decline at about 1100 s. The drop in $v(t)$ and $T(t)$ obeys power laws with critical exponents 0.17 ± 0.02 and 0.19 ± 0.04, respectively. This feature makes this process resemble phase transitions.

The discrepancy in t_c's, 1115 and 1180 s, determined for v and T, respectively, is due to the fact that T is measured as the average transmittance *behind the front* whereas v, the

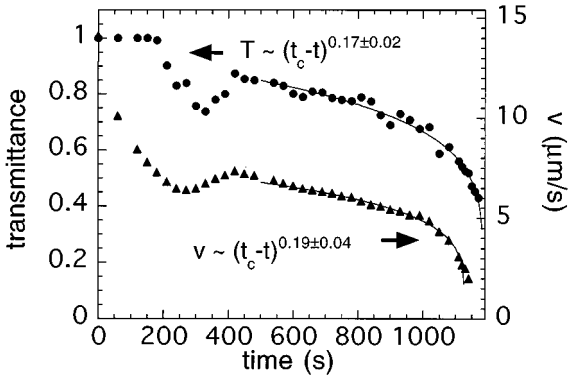

FIG. 7. Variation of the transmittance behind the front (filled circles) and the propagation velocity (triangles) vs time. Both transmittance and propagation velocity can be approximated by a power function with exponents 0.17 ± 0.02 and 0.19 ± 0.04, respectively.

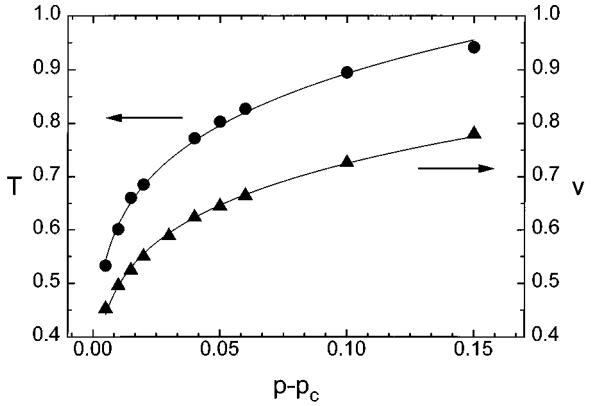

FIG. 8. Calculated transmittance (filled circles) and spreading velocity (triangles), vs spreading probability p.

propagation velocity, is related to the *front* itself. Therefore a time lag, Δt, of the order of $\Delta t \sim \Delta x/v$, occurs between the two t_c's, where Δx is the width of the front. Dividing $\Delta x \approx 200$ μm, the width of the corrosion front before the cessation of its propagation with the front velocity in the critical phase, being of the order of 4 μm/s, $\Delta t = 50$ s is obtained. The difference between the two t_c's (65 s) determined for $v(t)$ and $T(t)$, respectively, is in agreement with this estimate.

The evolution of the front can be interpreted within the framework of the spreading percolation model described. At the beginning growth sites coalesce and form a smooth corrosion front. Starting from 400 s the number of these active sites decreases. Using the language of the spreading percolation model, this corresponds to a steady decrease in p leading to gradual front roughening and finally to the cessation of the metal dissolution. Geometrical phase transition occurs when $p = p_c$.

D. Comparison of the experiment with model calculations

Although Fig. 7 indicates a steady decrease of the spreading probability in time, the $p(t)$ function cannot be retrieved from the experimentally determined $v(t)$ and $T(t)$ curves as long as $v(p)$ and $T(p)$ functions predicted by the model are not known [14,15]. In order to determine how v and T in the spreading bond percolation model vary with p, calculations have been carried out on a 3360×3360 square lattice. Cyclic boundary conditions were employed in the direction perpendicular to the front propagation. Each site on the lattice represented a 1 μm$\times$1 μm square on the ''Al film.'' A smooth front of active sites started to grow with *constant p* from one side of the lattice. The propagation velocity v was determined by fitting a straight line to the average position versus time curve. The transmittance was obtained by determining the ratio of empty sites to the total number of lattice sites. The relaxation period has been excluded from the determination of both v and T. This calculation was carried out for different p values, ranging from the bond percolation threshold on a 2D square lattice $p_c = 0.5$ to 0.8. Figure 8 shows that the same critical exponent, $\alpha = 0.17\pm0.02$, has been found for both $v(p)$ and $T(p)$. From the fact that the calculated $v(p)$ and $T(p)$ exponents are practically identical with the experimentally determined $v(t)$ and $T(t)$ exponents, we conclude that the gradual decrease of p can be approximated by a linear function of time and the time dependence of p can be extracted from the equality $v(t) = v[p(t)]$:

$$c_t(t_c - t)^{\alpha} = c_p[p(t) - p_c]^{\alpha}, \tag{2}$$

where $c_t = 0.248$, $c_p = 1.07$, $\alpha = 0.17$ were obtained from the fits shown in Figs. 7 and 8.

By rearranging Eq. (2) we obtain

$$p(t) = p_c + \left(\frac{c_t}{c_p}\right)^{1/\alpha}(t - t_c). \tag{3}$$

We can now apply Eq. (3) in the model calculation described above to reproduce the roughening transition observed experimentally. The unit time and the unit size employed in the calculation were determined as follows. The smallest velocity before the ramification of the front can be determined from Fig. 7. At about 180 s, $T(t)$ was still equal to 1, and the propagation velocity was 8 μm/s. As unit size we took 1 μm, the approximate width of the channels etched into the metal film, therefore the time unit was chosen to be 0.125 s. By means of the model calculation all the important features of the corrosion front propagation have been reconstructed.

Figure 9 shows the spatial distribution of the experimental and the calculated transmittances measured in the direction of front propagation. Apart from the slight deviation in the fall-off region, due to the large scatter of data in this domain, the agreement can be considered satisfactory. The calculated corrosion front along with the result of the box counting analysis is shown in Fig. 10. Scaling with the fractal dimension $D_f = 1.32\pm0.01$ was found between 10 and 1000 lattice units in excellent agreement with the experiment (cf. Fig. 4).

To explain why the front roughness increased with time we propose the following rather qualitative picture [12,16]. Metal dissolution (anodic reaction) occurs at active sites of the pit perimeter. The anodic current is represented by high current density j_a, flowing through a relatively small active surface area A_a. On the other hand, a large oxide covered surface area A_c is available for cathodic reactions taking

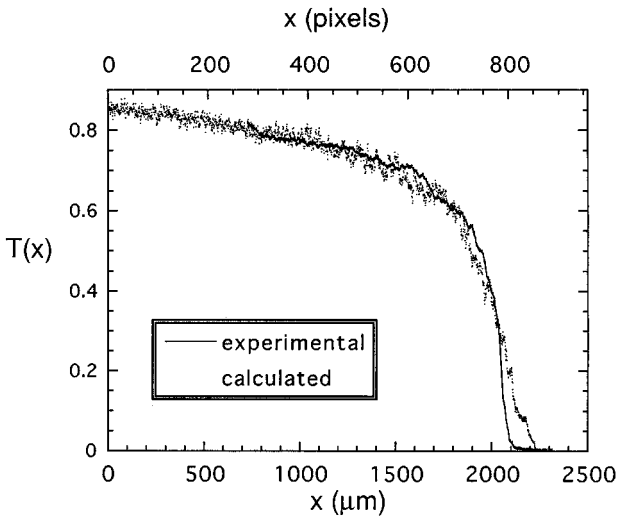

FIG. 9. Experimental (solid curve) and calculated (dotted curve) spatial distribution of the transmittance perpendicular to the growth front.

place at a much smaller rate, j_c, than j_a. As a result of open circuit conditions the anodic current and the cathodic current must be equal:

$$A_a j_a = A_c j_c . \tag{4}$$

Since A_c slowly decreases with the increase of pit size and j_c becomes quickly diffusion limited in dilute Fe^{3+} solutions [12], an upper limit exist for the anodic current. Once the limiting current has been reached, the active anodic area (active pit perimeter×film thickness) is further increased at the expense of diminishing anodic current density; the current thus remains constant. The decrease in the propagation velocity of the smooth front (cf. Fig. 7) indicates the decay of the dissolution current density j_a. Due to the fact that with

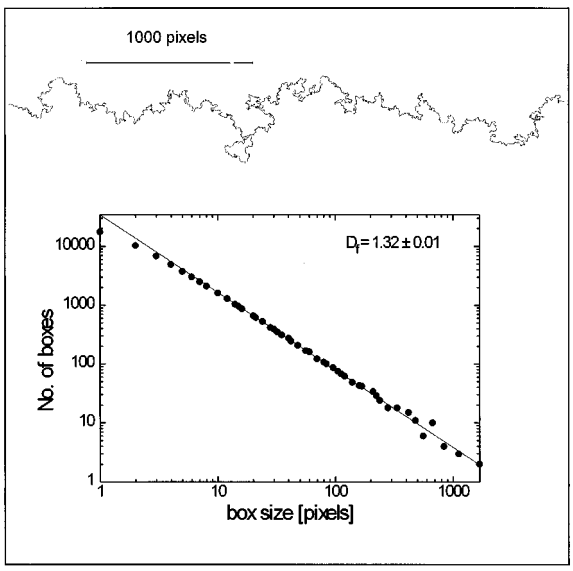

FIG. 10. Calculated corrosion front (upper section) and the result of box counting analysis. The fractal dimension of the simulated front ($D_f = 1.32 \pm 0.01$) is in agreement with the experiment (cf. Fig. 4).

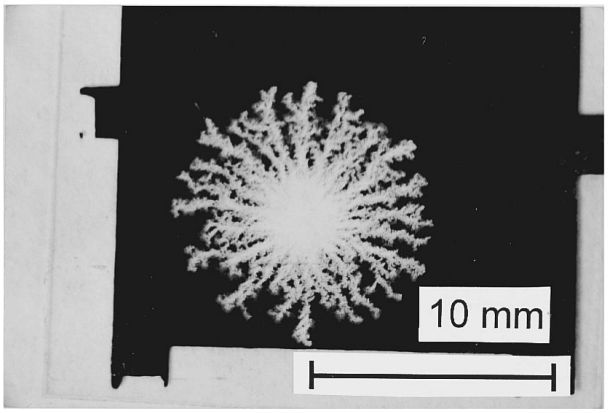

FIG. 11. Symmetric pit growth in Al thin film. Nucleation of the pit occurred far from the borders of the aluminum film.

the decline of j_a the local concentration of the aggressive corrosion products decreases the corrosion front becomes unstable and it will be partially passivated once the lower limit of the dissolution current density has been attained. Passivation leads to a decrease in the active surface, consequently the anodic current becomes smaller. As soon as the dissolution current density is stabilized at the critical value there remains only one way for the system to hold the corrosion current at the upper limit: a constant active anodic area must be maintained. Because the total length of the pit perimeter increases whereas the size of the total active area is constant, passivation occurs at certain spots of the active front.

Continuous spatial distribution in the degree of roughness along the pit perimeter was observed after the corrosion process was quenched by flooding the electrolyte cell with distilled water. In the direction of the arrow shown in Fig. 1 the density of active sites decreases from the densest possible case represented by a smooth front section to zero, where the corrosion process ceased and a fractal-like coastline was formed. That both temporal and spatial transition from smooth to fractal geometry occurred is probably because the pit nucleated close to the sample corner and pit growth was influenced by the asymmetry of the Al film around the evolving hole. This assumption is supported by a counterexample for symmetric pit growth under the same experimental conditions (see Fig. 11). In this case the pit started to grow in the middle of the sample. Passivation first occurred at randomly distributed spots on the initially circular pit perimeter when the upper limit of the corrosion current was attained. As time elapsed the pit grew ramified branches.

CONCLUSIONS

Under open circuit conditions, passivation and roughening of the initially smooth pit perimeter occurred because of the limit on the corrosion current imposed by the cathodic reactions. The local passivation was also influenced by the finite size of the specimen. The asymmetry of the aluminum film around the two-dimensional pit induced continuous *spatial* distribution in the morphology of the pit perimeter. When studying the evolution of a given section of the total perimeter we detected the *temporal* roughening of that particular part. Video images of the propagating corrosion front at high magnification indicated characteristic features of

spreading percolation phenomena. As a phenomenological model, spreading bond percolation with trapping successfully reproduced both the static and dynamic critical exponents characteristic of the roughening process.

We wish to stress that the interpretation of the roughening process observed is analogous to the concept of gradient percolation [17,18] introduced by Sapoval and co-workers. They considered the *site* percolation problem with a gradient in the occupation probability p. It is known that a self-similar front is formed, with the fractal dimension, $D_f=4/3$, corresponding to the fractal dimension [19] of the external perimeter [20] of the infinite percolation cluster at p_c. The concentration of the occupied cluster sites at the mean front position corresponds to p_c, and the width of the front is related to dp/dx.

In the present work we have shown that the roughening of the two-dimensional corrosion front can be understood within the framework of spreading *bond* percolation with trapping. A fractal coastline is formed if the spreading probability p associated with the evolving front decreases with time. Geometrical phase transition occurs when p becomes equal to p_c. The front obtained exhibits fractal properties with $D_f \cong 4/3$, corresponding to the connectivity of sites in the bond percolation problem. The upper cutoff, i.e., the front width, depends on dp/dt whereas the lower limit of scaling is determined by the width of the propagating channels etched in the aluminum layer.

ACKNOWLEDGMENTS

The author would like to thank B. Sapoval, M. Rosso, J-F. Gouyet, L. Nyikos, and R. Schiller for helpful discussions and J-P. Dallas for measuring the thickness of the aluminum film. This work was partly supported by the Hungarian Research Foundation OTKA under Contract No. 2981.

[1] T. Vicsek, *Fractal Growth Phenomena*, 2nd ed. (World Scientific, Singapore, 1992).
[2] *Dynamics of Fractal Surfaces*, edited by F. Family and T. Vicsek (World Scientific, Singapore, 1991).
[3] Z. Szklarska-Smialowska, Corrosion **27**, 223 (1971).
[4] J. M. Costa, F. Sagués, and M. Vilrassa, Corros. Sci. **32**, 665 (1991).
[5] B. Sapoval, M. Rosso, and J-F. Gouyet, in *The Fractal Approach to Heterogeneous Chemistry*, edited by D. Avnir (Wiley, New York, 1989).
[6] T. Nagatani, Phys. Rev. A **45**, R6985 (1992).
[7] P. Meakin, T. Jøssang, and J. Feder, Phys. Rev. E **48**, 2906 (1993).
[8] R. Reigada, F. Sagués, and J. M. Costa, J. Chem. Phys. **101**, 2329 (1994).
[9] T. Holten, T. Jøssang, P. Meakin, and J. Feder, Phys. Rev. E **50**, 754 (1994).
[10] G. S. Frankel, Corros. Sci. **30**, 1203 (1990).
[11] L. Balázs, L. Nyikos, I. Szabó, and R. Schiller, Fractals **1**, 416 (1993).
[12] L. Balázs and J-F. Gouyet, Physica A **217**, 319 (1995).
[13] R. Chandler, J. Koplik, K. Lerman, and J. Willemsen, J. Fluid Mech. **119**, 249 (1982).
[14] A. Bunde and S. Havlin, in *Fractals and Disordered Systems*, edited by A. Bunde and S. Havlin (Springer, Berlin, 1991), p. 51.
[15] The exact relation between v and p can be found in A. L. Ritzenberg and R. I. Cohen, Phys. Rev. B **30**, 4038 (1984); M. Barma, J. Phys. A **18**, L277 (1985).
[16] M. Hashimoto, S. Miyajima, and T. Murata, Corros. Sci. **33**, 885 (1992).
[17] B. Sapoval, M. Rosso, and J-F. Gouyet, J. Phys. (Paris) Lett. **46**, L149 (1985).
[18] J-F. Gouyet, M. Rosso, and B. Sapoval, in *Fractals and Disordered Systems*, edited by A. Bunde and S. Havlin (Springer, Berlin, 1991), p. 229.
[19] H. Saleur and B. Duplantier, Phys. Rev. Lett. **58**, 2325 (1987).
[20] Here the definition of the external perimeter is restricted to nearest-neighbor connections; see T. Grossman and A. Aharony, J. Phys. A **19**, L745 (1986); **20**, L1193 (1987).